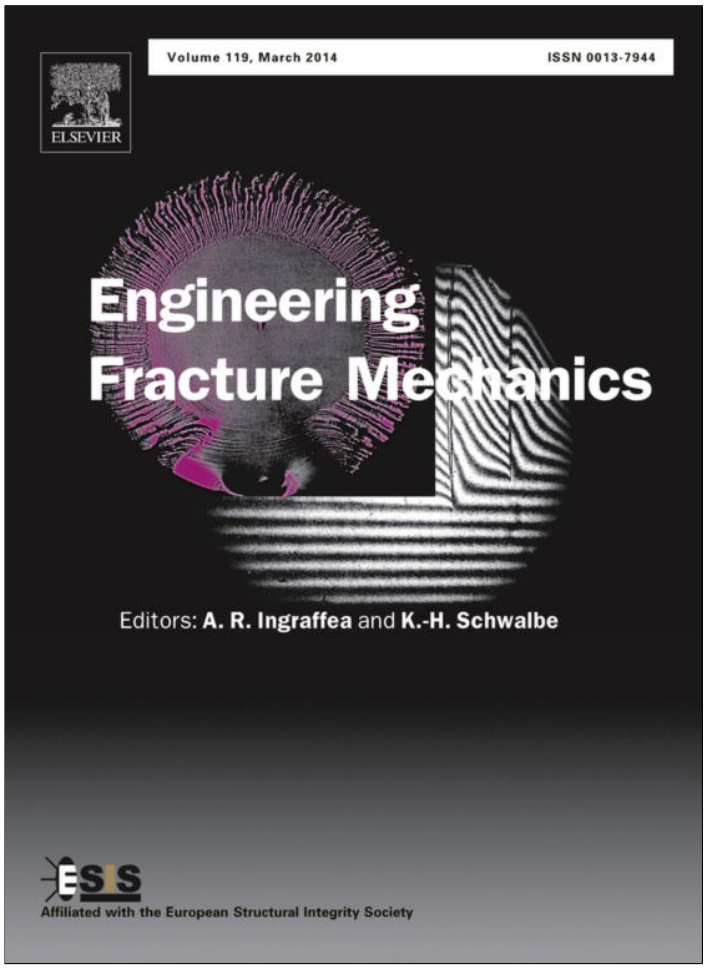

Engineering Fracture Mechanics 119 (2014) 21–28

Contents lists available at ScienceDirect

Engineering Fracture Mechanics

journal homepage: www.elsevier.com/locate/engfracmech

Discussion: Strength-to-fracture scaling in scratching

Ange-Therese Akono [a,b,*], Franz-Josef Ulm [b], Zdeněk P. Bažant [c]

[a] Department of Civil and Environmental Engineering, University of Illinois at Urbana-Champaign, Urbana, IL 61801, United States
[b] Department of Civil and Environmental Engineering, Massachusetts Institute of Technology, Cambridge, MA 02139, United States
[c] Department of Civil and Environmental Engineering, Northwestern University, Evanston, IL 60208-3109, United States

ARTICLE INFO

Article history:
Received 9 November 2013
Accepted 26 February 2014

Keywords:
Fracture mechanics
J-Integral
Ductile-to-brittle transition
Scratch tests

ABSTRACT

In their paper, Lin and Zhou (2013) add a new dimension to the scratch test analysis, challenging the applicability of Linear Elastic Fracture Mechanics to scratch tests. The question raised is how to integrate the three-dimensionality of scratch tests into the energetic Size Effect Law (SEL) formulated by Bažant for quasi-brittle materials. We show that Lin and Zhou's analysis, although relevant is incomplete, as it neglects the blade width, which is critical for the fracture property assessment. In return, if the blade width is properly taken into account, the SEL here proposed is a formidable means to ascertain the fracture toughness from scratching.

Published by Elsevier Ltd.

1. Introduction

Understanding the failure mechanisms of scratch tests continues to be a challenge in materials science and engineering, because of its impact on material characterization in many fields, ranging from strength property characterization of rocks [3,4,7,8], to adhesive properties of coatings [1,5] and damage and wear of metals [2] and polymers [6]. In its simplest form, the scratch test consists of driving a scratch tool across the surface of a weaker material as illustrated in Fig. 1. The challenge lies in rigorously connecting the forces (horizontal force F_T and vertical force F_V) and the penetration depth (d) measurements to the scratch tool geometry (width w, back-rake angle θ) and relevant material properties (strength σ_0, fracture energy $G_f = K_c^2/E^*$ or fracture toughness K_c), with two schools of thought existing:

The 'Strength'–School of thought links forces and geometry to strength properties, such as the scratch hardness [8]:

$$H_T = \frac{F_T}{A_{LB}} = \sigma_0 \times \Pi_S\left(\frac{d}{w}, \theta, \mu, \mu_i, \frac{\sigma_0}{E}, \frac{d}{(K_c/\sigma_0)^2}\right) \tag{1}$$

where A_{LB} is the horizontal projected load contact area, which in the case of a parallelepiped scratch blade is equal to the blade width w times the penetration depth d; while μ and μ_i stand for friction coefficients of material and interface, respectively. Detournay and coworkers [3,4,7] have substantially studied scratch testing on rocks with an inclined blade (Fig. 1 b) and reported a transition from ductile shearing to brittle micro-cracking at a penetration depth of 2 mm (Fig. 15 in [3]). Moreover in the ductile regime, an analytical model was developed that assumes the existence of two forces acting on the cutter: $\underline{F_c}$, acting on the inclined wedge, is associated to cutting processes, whereas $\underline{F_f}$ acting on the wear flat is associated to frictional dissipation. A specific intrinsic energy ε is introduced, which for a sharp cutter, and constant width, is akin to the

* Corresponding author. Address: 3108 Newmark Civil Engineering Laboratory, 205 N. Mathews Avenue., Urbana, IL 61801, United States. Tel.: +1 (217) 244 7917; fax: +1 217 333 9464.
E-mail address: aakono@illinois.edu (A.-T. Akono).

http://dx.doi.org/10.1016/j.engfracmech.2014.02.025
0013-7944/Published by Elsevier Ltd.

Nomenclature

A_{LB}	horizontally projected load-bearing contact area
B	Size Effect Law dimensionless coefficient
d	penetration depth
D_0	Size Effect Law transitional size
E	Young's modulus
F_T	scratch horizontal force
F_V	scratch vertical force
f'_t	tensile strength
G_f	fracture energy
H_T	scratch hardness
K_c	fracture toughness
p	scratch probe perimeter
θ	scratch blade back-rake angle
μ	material internal friction coefficient
μ_i	scratch blade-material interface friction coefficient
ν	Poisson's ratio
σ_0	material's strength

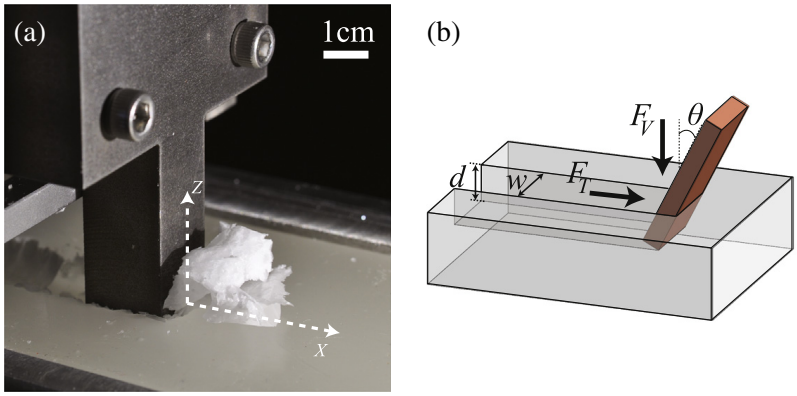

Fig. 1. Description of macroscopic scratch tests. (a) Scratch tests on paraffin wax with a straight blade: depending on the width w of the blade and on the depth d of penetration, chipping can be observed. (b) Schematic representation of a macro-scratch test with an inclined blade. F_V is the vertical force and F_T is the horizontal force.

scratch hardness. Assuming that $\underline{F}_c$ and $\underline{F}_f$ maintain constant directions characterized by the parameters ζ and μ_i, respectively, the specific intrinsic energy ε is related to the vertical and horizontal forces as well as the width of the blade, w, and the depth of penetration, d (for details, see [7], Eq. (1)). An extensive series of testing performed on hundreds of rock specimens with a standard cutter width $w = 10$ mm suggests an empirical correlation between the specific intrinsic energy ε and the uni-axial compressive strength σ_0, and between the interface friction coefficient μ_i and the rock's internal friction coefficient $\mu = \tan\phi$. However, further investigation [7] revealed that both the specific intrinsic energy ε and interface friction coefficient μ_i also depend on the cutter geometry. For purpose of illustration, Fig. 2 displays the values of the intrinsic specific energy ε and of the interface friction coefficient μ_i for scratch tests performed on six materials: paraffin wax, cement paste, A-51w, B-4w and B-12 w. The original scratch test data have been presented in [12,14,17]. All six specimens exhibit similar trends: the intrinsic specific energy ε decreases with blade width w, whereas the interface friction coefficient μ_i strongly depends on the blade width w.[1] Richard et al. rationalize the variation of the intrinsic specific energy ε with the blade width w by introducing a shear-induced dilatation mechanism, which in turn leads to the conclusion that ductile failure prevails for large blade widths $w \geqslant 10$ mm and small penetration depths d. However, as can be seen on Fig. 3, the linear scaling between the horizontal force F_T and the projected horizontal contact area $A_{LB} = wd$, which is a major underlying assumption of the strength-scratch model, is valid mainly for small blade widths – here $w = 2.5$, 5 mm.

The 'Fracture'–School of Thought departs from the premise that the particular scaling of strength properties with the blade width is related to fracture processes; that is ([13]):

[1] It should be noted that the dependence of the interface friction coefficient μ_i on w violates the principle of Amonton's laws of friction, according to which the friction coefficient is thought to be independent of the contact area.

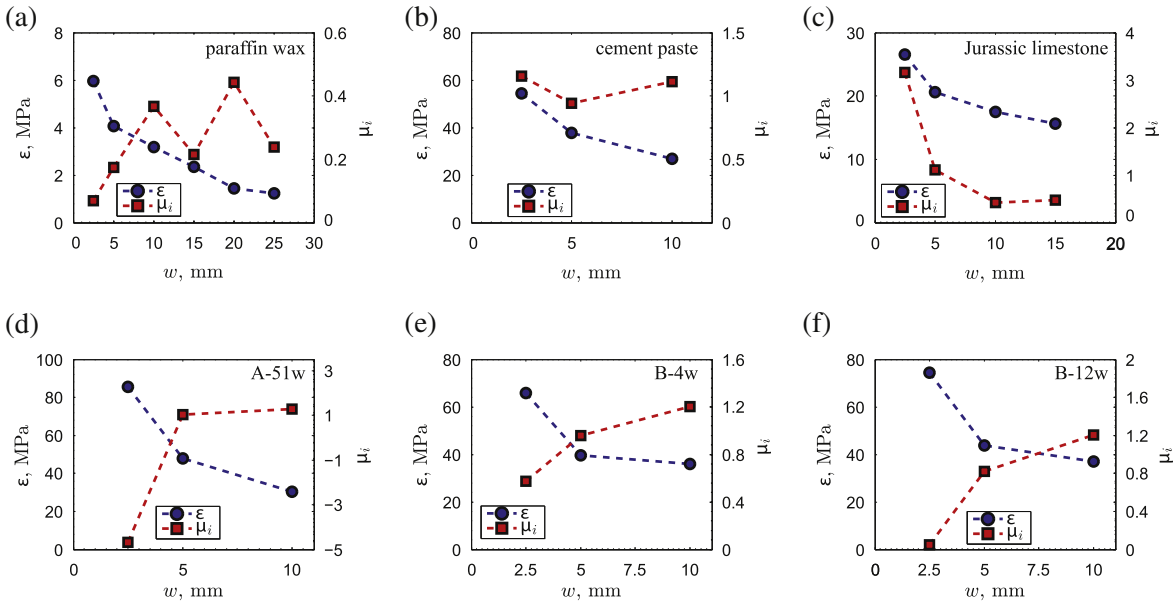

Fig. 2. Influence of cutter width w on the intrinsic specific energy ε and the interface friction coefficient μ_i. Analysis of the original scratch test data presented in [12,14,17]. For a given material and for a given blade width w, the intrinsic specific energy ε and the interface friction coefficient μ_i were calculated independently using respectively Eqs. (1) and (4) in [7]. In the tests, six blade widths $w = [2.5, 5, 10, 15, 20, 25]$ mm are employed. (a) Paraffin wax. (b) Cement paste with $w/c = 0.44$. (c) Jurassic limestone. (d) A-51w. (e) B-4w. (f) B-12w.

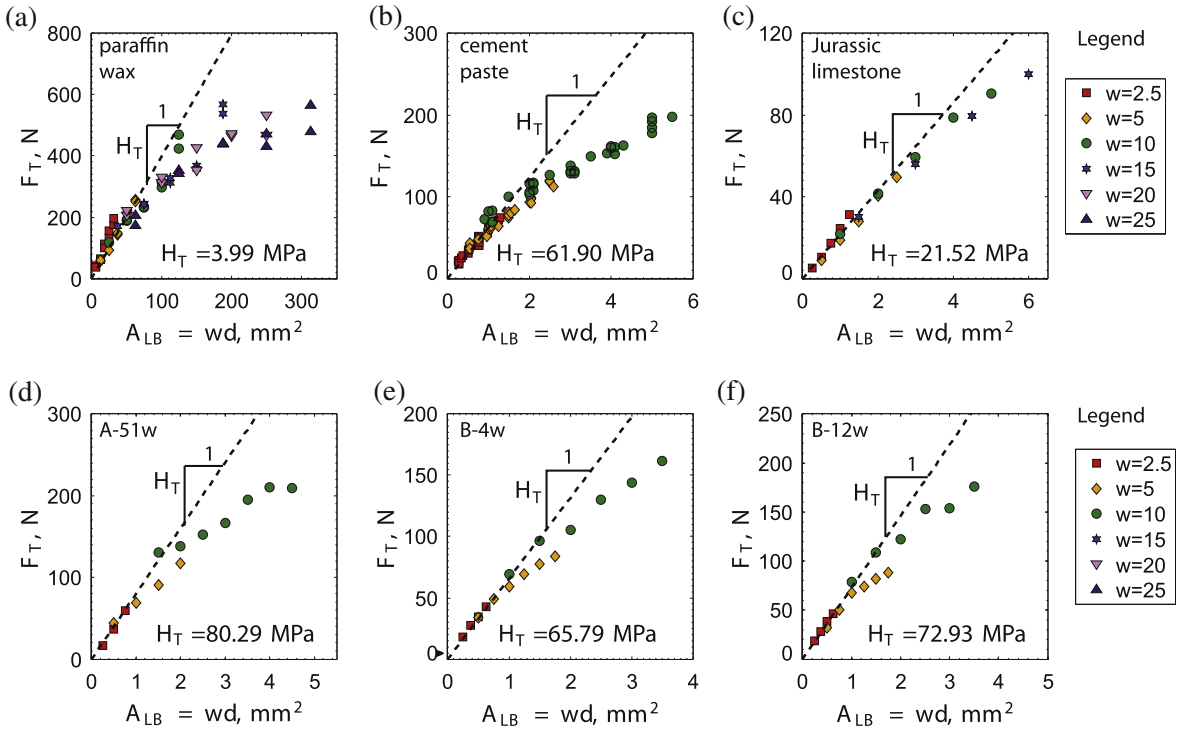

Fig. 3. Strength scaling of scratch tests for different geometries (straight vs. inclined blade), various blade widths ($w = [2.5, 5, 10, 15, 20, 25]$ mm) and various penetration depths w. Analysis of the original scratch test data presented in [12,14,17]. The scratch hardness H_T is the initial slope of the curve (F_T vs. $wA_{LB} = wd$). In particular, the linear scaling between the horizontal scratch force F_T and the projected horizontal contact area A_{LB} is valid only for small blade widths w. (a) Paraffin wax. (b) Cement paste with $w/c = 0.44$. (c) Jurassic limestone. (d) A-51w. (e) B-4w. (f) B-12w.

$$\frac{F_T}{\sqrt{2pA_{LB}}} = K_c \times \Pi_F\left(\frac{w}{d}, \theta, \frac{a}{w}, \mu, \mu_i, \frac{\sigma_0}{E}, \frac{w}{(K_c/\sigma_0)^2}\right) \tag{2}$$

where p is the perimeter of the scratch probe (i.e. $p = w(1 + 2d/w)$ for the rectangular blade), a is the horizontal crack length ahead of the probe (as typically observed in scratch tests; see Fig. 4a). Neglecting friction effects, the analytical model devel-

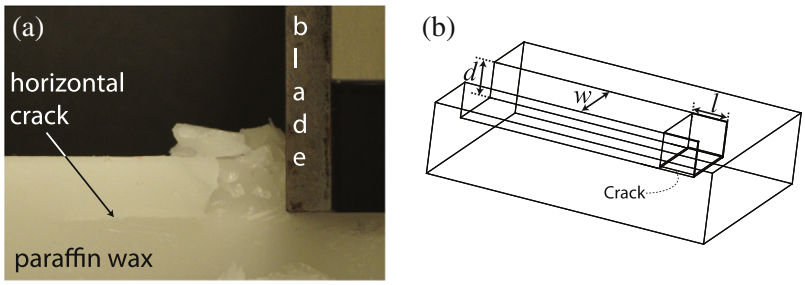

Fig. 4. (a) Presence of a horizontal propagating crack during scratch testing experiments performed on paraffin wax with a straight steel blade. (b) Idealized crack geometry during scratch testing: the crack front is assumed to be three-dimensional, with a rectangular cross-section, and characterized by a length ℓ. w is the blade width and d is the penetration depth.

oped in [14] employs a J-Integral method to evaluate the energy release, for scratch tests with an infinite width $\left(w/d \to \infty, a/w \to 0, w/(K_c/\sigma_0)^2 \to \infty, \lim_{w/d\to\infty}\sqrt{2pA_{LB}} = w\sqrt{2d}\right)$, for which $\lim_{w/d\to\infty} \Pi_F = \mathcal{F}(\theta)$, where $\mathcal{F}(\theta) = 1$ for a straight blade $(\theta = 0)$ –a solution previously obtained by Cherepanov and Cherepanov [21][2]–, and $\mathcal{F}(\theta) = F_T/F_{eq}$ with $F_{eq} = F_T\sqrt{1 + 3/5(F_V/F_T)^2}$ for an inclined blade $(\theta > 0)$, for which both horizontal and vertical stresses at the blade-material interface contribute to the energy release rate (for details see [14], and for a generalization to other scratch probe geometries [13,15]). By means of finite element calculations, in which mode I and mode II fracture modes were investigated, the previous solution was found to be highly accurate for back-rake angles $\theta \in [0, 20^\circ]$ and interface friction coefficients $\mu_i \leqslant 0.2$ [20].

Lin and Zhou [9] add a new dimension to the discussion by applying the energetic Size Effect Law (SEL) [10,11] to scratch testing. The idea is appealing, as SEL is able to bridge – under well defined self-similarity conditions – between strength and fracture theories in the form:

$$\sigma_N = \frac{Bf_t'}{\sqrt{1 + D/D_0}} \tag{3}$$

where f_t' is the tensile strength, B is a dimensionless constant and D_0 is the transitional size representing the shift from ductile to brittle failure. Both B and D_0 depend on the fracture properties of the material and on the geometry of the structure. Lin and Zhou choose the penetration depth $d \equiv D$ as the structure size, and define the nominal stress σ_N as the ratio of the average peak force to the projected horizontal contact area $A_{LB} = wd$. For scratch test results on rock with a constant width $w = 10$ mm, they were able to reconstruct the evolution of the nominal stress with the general Size Effect Law: in particular, based on the calculated value of the transitional size $D_0 = 1.67$ mm, Lin and Zhou ruled out the predominance of fracture processes during conventional macroscopic scratch testing – with penetration depths less than 10 mm – and concluded that macroscopic scratch testing could not be used for fracture determination purposes. Moreover, in the brittle scratch testing regime, using digital photography and finite element simulations, they showed evidence of complex fracture processes involving several cracks with varying orientations, which leads them to question the validity of a previously developed scratch fracture model that assumes a single horizontal propagating crack [12,14].

That macroscopic scratch test data can be reproduced using the energetic Size Effect Law is remarkable, as it provides an additional confirmation of the presence of both ductile and brittle failure mechanisms at work during scratch tests. The question is how to articulate the three-dimensional character of scratch tests; and how to practically adjust macroscopic scratch tests so as to favor a specific mode of failure? This is in short the focus of this discussion.

2. Energetic Size Effect Law for macroscopic scratch tests with variable blade width

For further developments it is instructive to recall some of the fundamentals of SEL, bridging between the strength asymptote and the LEFM asymptote. First, the strength asymptote, relevant for perfectly plastic materials, is defined by a constant nominal strength, σ_N, independent of the structure size, D. Second, the Linear Elastic Fracture Mechanics (LEFMs) asymptote, relevant for perfectly brittle materials, predicts a linear scaling between the nominal strength and the square root of the structure characteristic length, with $\sigma_N \sim D^{-1/2}$, due to the fact that the potential energy stored within a volume of material is dissipated upon crack propagation along a surface area. Quasi-brittle materials exhibit an intermediate behavior due to the presence of a large nonlinear softening zone – also called Fracture Process Zone – characterized by progressive damage and strain-softening behavior due to various phenomena such as distributed cracking, frictional slips or void coalescence. Examples of quasi-brittle materials include cementitious materials, rocks, tough ceramics, bones, sea ice, fiber com-

[2] The main difference with the more general solution derived in [14] is that Cherepanov and Cherapanov [21] consider the scratch test to be a Mode II fracture test. FE simulations, however, show that the scratch test involves both Mode I and Mode II, and that the mode angle K_{II}/K_I depends on the back-rake angle θ; with $|K| = \sqrt{K_I^2 + K_{II}^2} = F_{eq}\Big/\left(w\sqrt{2d}\right)$.

posites and wood. Due to the energy release caused by stress redistribution upon micro-cracking, quasi-brittle materials exhibit a structural size effect in which the nominal strength decrease when the structure size is increased. The asymptotic approximation represented by Eq. (3) was initially proposed in 1984 [16], in order to capture the strength scaling of concrete, rocks and metals over a wide range of length-scales, thus bridging the gap between strength theories and Linear Elastic Fracture Mechanics. Thirty years later, this law has been extensively applied to model the failure behavior of materials in several fields of science and engineering ranging from the design of concrete structures to the fracture of sea ice and the size-dependence of microscopic hardness in metals. In what follows, we will formulate the energetic Size Effect Law for macroscopic scratch testing.

Our starting point is the expression of the energy release rate for an infinite blade width, reading [14] $\mathcal{G} = \lim_{w\to\infty}(E' F_T^2/(pA_{LB})II_F^{-2}) = E' F_{eq}^2/(2w^2 d)$, with $E' = E/(1-\nu^2)$ the plane strain modulus; where we recall that F_{eq} is equal to F_T for a straight blade ($\theta = 0$) and $F_{eq} = \sqrt{F_T^2 + 3/5F_V^2}$ for an inclined blade ($\theta > 0$). Knowing the asymptotic solution for an infinite width, we can express the energy release rate for scratch tests with a finite blade width, considering the additional dimensionless quantities in Eq. (2):

$$\mathcal{G} = \frac{1}{E'}\frac{F_{eq}^2}{2w^2 d}\mathcal{J}\left(\frac{c_f}{d}, \frac{a}{c_f}, \frac{w}{c_f}\right) \tag{4}$$

where $c_f = (K_c/f_t')^2 = E' G_f/(f_t')^2$ characterizes the size of the plastic process zone. Defining the nominal strength as the ratio of the equivalent force to the projected horizontal contact area, $\sigma_N = F_{eq}/(wd)$, and applying the fracture criterion ($\mathcal{G} \equiv G_f$, with $G_f = K_c^2/E'$ the fracture energy), we can rewrite Eq. (4) as:

$$\sigma_N = \frac{K_c\sqrt{2}}{\sqrt{d\mathcal{J}\left(\frac{c_f}{d}, \frac{a}{c_f}, \frac{w}{c_f}\right)}} \tag{5}$$

In turn, the function $\mathcal{J}$ can be expanded for small variations of the ratio c_f/d around zero; that is, $\mathcal{J} \approx g_0^w + g_1^w\, c_f/d$; where $g_0^w = \mathcal{J}(0, a/c_f, w/c_f)$ and $g_1^w = \mathcal{J}_{,x_1}(0, a/c_f, w/c_f)$ respectively stand for the values of $\mathcal{J}$ and its partial derivative with respect to the first argument around the origin ($c_f/d \to 0$). From this expansion, it is readily recognized that g_0^w and g_1^w depend on the blade width w. Inserting this approximation into Eq. (5), we can rewrite the nominal strength as:

$$\sigma_N = \frac{K_c\sqrt{2}}{\sqrt{dg_0^w + g_1^w c_f}} = \frac{K_c\sqrt{2}\Big/\sqrt{g_1^w c_f}}{\sqrt{1 + \frac{g_0^w}{g_1^w c_f}d}} \tag{6}$$

Therefore, we obtain the classical form of the Size Effect Law given in Eq. (3) with the asymptotic fracture parameters B^w and D_0^w given by:

$$B^w f_t' = \frac{K_c\sqrt{2}}{\sqrt{g_1^w c_f}}; \quad D_0^w = \frac{g_1^w}{g_0^w}c_f \tag{7}$$

This derivation of the energetic Size Effect Law holds provided we assume (i) a constant fracture energy –independent on the crack orientation – (ii) a smooth dependence of the energy release rate upon the crack length, the penetration depth and the blade width, and (iii) a positive geometry ($g_1^w > 0$); meaning that the fracture toughness decreases with the crack length at constant nominal stress[3]. The resulting expression (6) is the same used by Lin and Zhou [9], when letting $D \equiv d$; yet with one subtle, but important addition. From the expansion (5) for finite scratch widths, it is recognized that both, $B^w = \sqrt{2/g_1^w}$ and $D_0^w = g_1^w/g_0^w\, c_f$ depend on both the material's fracture properties and blade width w. This is due to the fact that the SEL of the form (3) holds strictly for two-dimensional self-similar structures (same width, w), and hence the quantities B^w and D_0^w need to be recalculated for each scratch width. Moreover, from the analytical solution at infinite width ($w \to \infty, g_0^w \to 1$), we can estimate the fracture toughness, knowing the SEL asymptotic fracture parameters for very large blade widths w:

$$K_c^{SEL} = B^w f_t' \frac{\sqrt{D_0^w}}{\sqrt{2}} \quad (w \to \infty) \tag{8}$$

[3] From Eq. (6) the fracture toughness can be expressed as a function of the nominal strength:

$$K_c = \frac{\sigma_N}{\sqrt{2}}\sqrt{g_0^w d}\left[1 + \frac{g_1^w}{g_0^w}\frac{c_f}{d}\right]^{-1/2} \approx \frac{\sigma_N}{\sqrt{2}}\sqrt{g_0^w d}\left[1 - \frac{1}{2}\frac{g_1^w}{g_0^w}\frac{c_f}{d}\right]$$

In particular, the fracture process is stable provided both g_0^w and g_1^w are positive.

3. Does blade width matter?

The Size Effect Law (SEL) formulated above was applied to analyze the scratch tests results of six materials including paraffin wax, four different cement pastes, and Jurassic limestone. The original scratch data can be found elsewhere [12,14,17]. Macroscopic scratch tests were performed on all six materials. A straight blade ($\theta = 0$) was used on paraffin wax at a constant velocity of 1.7 mm/s; whereas an inclined blade ($\theta = 15^\circ$) at a constant velocity of 10 mm/s was used for the remaining five materials. Six blade widths $w = [2.5,\ 5,\ 10,\ 15,\ 20,\ 25]$ mm were used on paraffin wax with penetration depths ranging from 2.5 to 12.5 mm whereas a maximum of four blade widths $w = [2,5,\ 5,\ 10,\ 15]$ mm were used on the other materials with penetration depths ranging from 0.1 to 0.55 mm so that the width-to-depth ratio, w/d, spanned almost two orders of magnitude in all cases.

For a given material and a given blade width, the SEL constants were calculated according to the method outlined in [10] (Section 6.3.2). In particular, a linear regression was carried out between $(f_t')^2/\sigma_N^2$ and d, and parameters B^w and D_0^w were calculated from the fitted linear regression coefficients. In doing so, we considered the link between the tensile strength f_t' and the scratch hardness from Bard and Ulm [8]'s closed-form lower-bound strength solution for scratch hardness (1), for a cohesive–frictional materials:

$$H_T = \left.\frac{dF_T}{d(wd)}\right|_{w/d=0} = f_t' \times \Pi_S'(\mu = \tan\varphi, \theta) \tag{9}$$

For instance, for a Mohr–Coulomb type material, $\Pi_S'(\mu,\theta)$ reads as:

$$\Pi_S'(\mu,\theta) = \frac{(1+\sin\varphi)\left(1-\sin^2\theta\right)}{1-\sin\varphi\cos^2\theta - \cos\varphi\sin\theta\sqrt{1+(\tan\varphi\sin\theta)^2}} \tag{10}$$

Furthermore, the fracture toughness K_c is evaluated by applying the model developed in [12,14], considering the asymptotic value $K_c = F_{eq}/(w\sqrt{2d})$ for large width-to-depth w/d ratios. Given Eq. (9), the linear regression $Y = A^w X + C^w$ is carried out for $X = d,\ Y = \sigma_N^{-2} = [F_{eq}/(wd)]^{-1/2}$, and provides values for $B^w = \Pi_S'(C^w)^{-1/2}/H_T$, and $D_0^w = C^w/A^w$; so that the SEL can be evaluated independently for different scratch widths w in the dimensionless form:

$$\frac{\sigma_N}{B^w f_t'} = \frac{\sigma_N}{C_w^{-1/2}} = \frac{1}{\sqrt{1+d/D_0^w}} \tag{11}$$

Furthermore, with K_c and H_T directly measured from the scratch tests carried out with different blade widths w, the characteristic size of the plastic process zone, $c_s = c_f/\Pi_S'^2 = (K_c/H_T)^2$, can be determined close to a multiplying constant $\Pi_S'^2$ which only depends on the material internal friction coefficient ϕ and the blade back-rake angle θ. In return, the dimensionless expression Π_S' does not depend on the blade width w or on the penetration depth d.

Fig. 5 displays for each material the dimensionless quantity $\sigma_N/(B^w f_t')$ as a function of d/D_w^0 as well as the evolution of the characteristic size D_w^0 with the blade width w; the numerical value of D_0^w and B^w are listed in Table A A.2 of the appendix. The results show that the SEL remains valid for different blade widths if the constants, B^w and D_0^w, are correctly evaluated for each blade width w. Specifically, for small widths, the data points come close to the plasticity theory asymptote. This along with the linear correlation between the scratch horizontal force F_T and the projected horizontal contact area $A_{LB} = wd$ observed for small blade widths (Fig. 3) confirms that for small widths ($w < 10\ c_f$) and for small width-to-depth w/d ratios, scratch tests are strength-driven. In return, as the blade width w increases, the data points approach the LEFM asymptote, where fracture processes are predominant and characterized by a linear correlation between $w\sqrt{2d}$ and F_{eq}, as we found earlier [14]. This suggests that the SEL in the dimensionless form (11) can be used as an appropriate criterion to distinguish between strength-dominated and fracture-driven scratch tests. Otherwise said, in contrast to Lin and Zhou's proposal [9], it is the blade width w, and not the scratch depth d alone, that governs the transition from ductile failure to brittle fracture in the scratch test.

Moreover, we enforce a quantitative convergence criterion, $d/D_0^w \geqslant 9.3$, that ensures that the relative uncertainty between the Size Effect Law and the LEFM asymptote is less than 5%. In other words for values of the penetration depth d greater than 9.3 times the transitional depth D_0^w, fracture processes are predominant and LEFM modeling can be used to estimate the fracture toughness. Herein convergence is reached for paraffin wax, cement paste, A-51w and B-12w as can be seen on Figs. 5(a), (b), (d) and (f). In return, Table 1 contrasts the estimates of the fracture toughness provided by the Size Effect Law (Eq. (8)) and our scratch fracture model. For all materials for which convergence towards a fracture-driven state is achieved, the predictions from both methods, Size Effect Law and scratch fracture model, agree perfectly within the experimental error bounds. However, there is some discrepancy for Jurassic limestone and B-4w for which the fracture dissipation does not become predominant as shown in Figs. 5(c) and (e). Moreover, as noted in [12,14], for paraffin wax and cement paste, the fracture toughness predicted by scratch tests is in excellent agreement with conventional fracture testing methods such as three-point bending tests on single-edge notched specimens or wedge splitting tests. This is further confirmation that our analytical scratch test fracture model enables to probe true material fracture properties, provided that the blade width w and the width-to-depth w/d ratios are large enough.

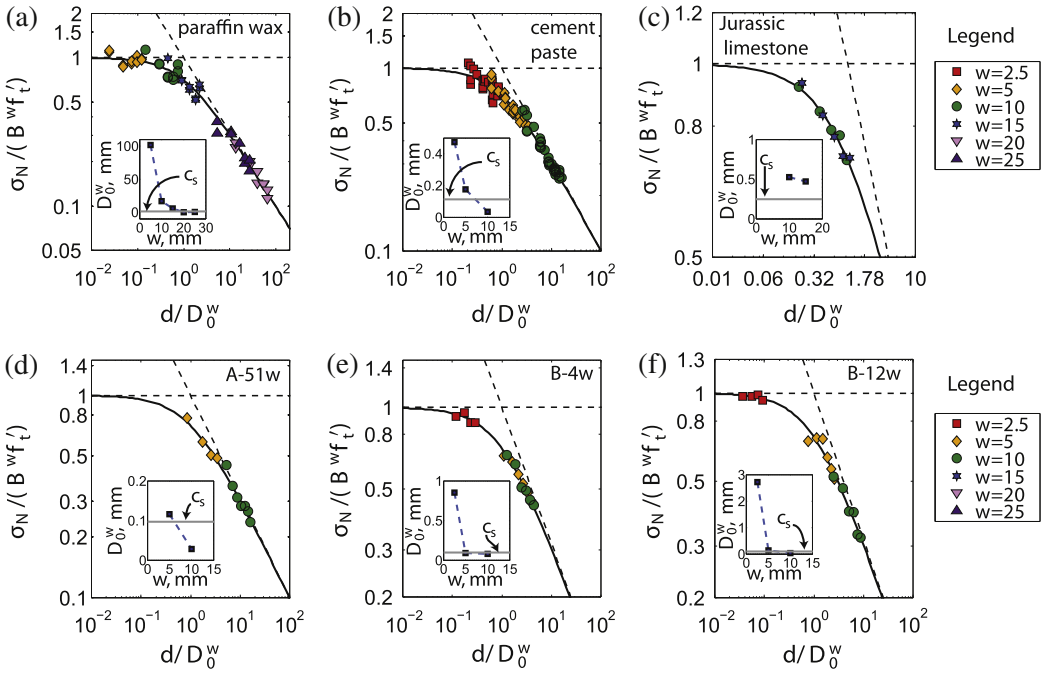

Fig. 5. Application of Bažant's Size Effect Law to scratch tests for different geometries (straight vs. inclined blade), various blade widths ($w = [2.5, 5, 10, 15, 20, 25]$ mm) and various penetration depths d. σ_N is the nominal strength, f_t' is the tensile yield strength; B^w and D_0^w are the asymptotic fracture parameters that are calculated independently for each material and for each blade width w. $c_s = (K_c/H_T)^2$ yields an estimate of the material plastic process zone; with K_c the scratch fracture toughness and H_T the scratch hardness. Analysis of the original scratch test data presented in [12,14,17]. (a) Paraffin wax. (b) Cement paste with w/c = 0.44. (c) Jurassic limestone. (d) A-51w. (e) B-4w. (f) B-12w.

Table 1
Fracture toughness determination: comparison of the scratch test Size Effect Law and scratch test fracture model predictions with that of conventional fracture testing methods. K_c^{SEL} is evaluated by applying Eq. (8) to the largest blade width. K_c^F is the asymptotic value of $F_{eq}\Big/\left(w\sqrt{2d}\right)$ for large width-to-depth w/d ratios. The original scratch test data of the materials analyzed here can be found in [12,14,17]. The fracture toughness of paraffin wax was determined independently using three-point bending tests on single-edge notched specimens.

	Scratch SEL method K_c^{SEL}, MPa $\sqrt{m}$	Scratch fracture model K_c^F, MPa $\sqrt{m}$	Classical fracture testing K_c, MPa $\sqrt{m}$
Paraffin wax	0.14	0.14	0.15 ± 0.01 [12]*
Cement paste	0.67	0.66 ± 0.05	0.62–0.66 [18,19]
Jurassic limestone	0.56	0.34 ± 0.01	
A-51w	0.82	0.79 ± 0.11	
B-4w	0.74	0.65 ± 0.07	
B-12w	0.78	0.70 ± 0.08	

It is in this light, that it is worthwhile to re-analyze Lin and Zhou's argument. After applying the SEL to scratch tests data with a single width on a Carthage marble sample, they found $D_0^w = 1.67$ mm; and conclude that LEFM is not to applicable to scratch tests with penetration depths d less than 20 mm. While there is no doubt that their value of the SEL transitional size $D_0^w = 1.67$ mm is relevant, it appears to us that this particular size is only representative for the specific blade width and material investigated – but cannot be postulated to be relevant for other scratch widths or for other quasi-brittle materials. In fact, as Fig. 5 and Table A.2 illustrate, the SEL transitional size D_0^w decreases with the blade width. For instance, for paraffin wax (Fig. 5a), D_0^w spans more than two decades from $D_0^w = 101$ mm for $w = 5$ mm to $D_0^w = 0.46$ mm for $w = 25$ mm. That is, while Lin and Zhou's data for a single width certainly does not approach the LEFM asymptote (similar to our Jurassic limestone data set, Fig. 5c), their generalization appears flawed to us, as they did not account for the critical third dimension of scratch tests, that is the scratch width w, in the application of SEL. Otherwise said, when properly scaled by a range of blade widths, covering a large enough width-to-depth ratio w/d, the scratch test is a highly accurate test to determine fracture properties.

In summary, while we reject Lin and Zhou's conclusions, we are grateful for their suggestion to employ SEL to quantitatively position scratch tests between the strength asymptote (for small contact areas) and the LEFM asymptote (for large widths w and width-to-depth w/d ratios); and determine accordingly strength or fracture properties. Moreover, the proposed SEL approach allows a direct determination of the fracture toughness, which is strictly equivalent to the method proposed in our previous work.

Table A.2
The Size Effect Law parameters: A^w, C^w, B^w and D_0^w were calculated for each material and for each blade width. H_T is the scratch hardness as defined by Eq. (9) and f_t' is the tensile strength. R^2 is the coefficient of correlation. The method is applied to the six materials presented previously and for which the original scratch test data can be found in [12,14,17].

w (mm)	$H_T^2A^w$ (mm^{-1})	$H_T^2C^w$ (no unit)	R^2 (no unit)	B^wf_t' (MPA)	D_0^w (mm)
Paraffin wax					
5	0.0089	0.90	0.044	4.20	101.65
10	0.054	0.91	0.28	4.19	16.64
15	0.13	0.75	0.55	4.60	5.60
20	0.31	0.058	0.91	16.63	0.19
25	0.44	0.20	0.86	8.87	0.46
Cement paste					
2.5	1.05	0.50	0.46	87.76	0.47
5	2.44	0.43	0.88	94.56	0.18
10	4.17	0.14	0.95	163.32	0.034
Jurassic limestone					
10	8.99	4.71	0.97	28.52	0.52
15	12.09	5.70	0.95	25.94	0.47
A-51w					
5	3.30	0.38	0.95	129.92	0.12
10	4.77	0.13	0.95	219.38	0.028
B-4w					
2.5	0.75	0.64	0.59	82.49	0.85
5	3.61	0.33	0.99	114.39	0.092
10	3.94	0.32	0.96	116.92	0.080
B-12w					
2.5	0.29	0.78	0.40	82.57	2.72
5	3.51	0.47	0.85	106.63	0.13
10	4.45	0.18	0.95	173.89	0.040

Appendix A. Size Effect Method: Application to Scratch Tests

Table A.2 lists the numerical values of the asymptotic fracture parameters calculated from the Size Effect Law applied to the six materials presented previously in [12,14,17]. For each material and for each blade width w, a linear regression was performed between the penetration depth $X = d$ and the inverse of the square of the nominal strength $Y = \sigma_N^{-2} = [F_{eq}/(wd)]^{-1/2}$; $Y = A^wX + C^w$. The transitional size was then calculated from $D_0^w = C^w/A^w$ and the second SEL parameter was calculated from $B^wf_t' = 1\Big/\sqrt{C^w}$ (see A.2).

References

[1] Ollendorf H, Schneider D. A comparative study of adhesion test methods for hard coatings. Surf Coat Technol 1999:113, 86–102.
[2] Wredenberg F, Larrson P-L. Scratch testing of metals and polymers: experiments and numerics. Wear 2009;266:76–83.
[3] Richard T, Detournay E, Drescher A, Nicodeme P, Fourmaintraux D, The scratch test as a means to measure strength of sedimentary rocks. In: SPE/ISRM 47196, 1998.
[4] Schei G, Fjær E, Detournay E, Kenter CJ, Fuh GF. The Scratch Test: An Attractive Technique for Determining Strength and Elastic Properties of Sedimentary Rocks. In: SPE 63255, 2000.
[5] Randall NX, Favaro G, Frankel CH. The effect of intrinsic parameters on the critical load as measured with the scratch test method. Surf Coat Technol 2001;137(2–3):146–51.
[6] Briscoe BJ, Evans PD, Pelillo E, Sinha SK. Scratching maps for polymers. Wear 1996;200:137–47.
[7] Richard T, Dagrain F, Detournay E. Rock strength determination from scratch tests. Engng Geol 2012;147–148:91–100.
[8] Bard R, Ulm F-J. Scratch hardness-strength solutions for cohesive-frictional materials. Int J Numer Anal Methods Geomech 2012;36:307–26.
[9] Lin J-S, Zhou Y. Can scratch tests give fracture toughness? Engng Fract Mech 2013;109:161–8.
[10] Bažant Z, Planas J. Fracture and size effect in concrete and other quasibrittle materials. Boston: CRC Press; 1997.
[11] Bažant Z. Scaling of structural strength. London: Hermes Penton Science; 2002.
[12] Akono A-T, Reis PM, Ulm F-J. Scratching as a fracture process: from butter to Steel. Phys Rev Lett 2011;106:4302.
[13] Akono A-T, Ulm F-J. Fracture scaling relations for scratch tests of axisymmetric shape. J Mech Phys Solids 2012;60:379–90.
[14] Akono A-T, Ulm F-J. Scratch test model for the determination of fracture toughness. Engng Fract Mech 2011;78:334–42.
[15] Akono A-T, Randall NX, Ulm F-J. Experimental determination of the fracture toughness via microscratch tests: application to polymers. Ceram Met 2012:485–93.
[16] Bažant Z. Size effect in blunt fracture: concrete, rock, metal. J Engng Mech-ASCE 1984;110:518–35.
[17] Ulm F-J, Simon J. The scratch test for strength and fracture toughness determination for oil well cements cured at high temperature and pressure. Cem Concr Res 2011;41:942–6.
[18] Hu XZ, Wittmann F. Size effect on toughness induced by crack close to free surface. Engng Fract Mech 2000;65(2–3):209–11.
[19] Cotterell B, Mai Y-W. Crack growth resistance curve and size effect in the fracture of cement paste, 1987;22:2734–38.
[20] Akono A-T. Scratch test: a new way of evaluating the fracture toughness of materials. Master thesis, Massachusetts Institute of Technology; 2011.
[21] Cherepanov AG, Cherepanov GP. Cutting resistance of rocks. Strength Mater 1990;22.11:1626–45.